

Supplementary Material for “Non-Hermitian skin effect in magnetic systems”

Kuangyin Deng^{1,*} and Benedetta Flebus^{1,†}

¹*Department of Physics, Boston College, 140 Commonwealth Avenue,
Chestnut Hill, Massachusetts 02467, USA*

In this Supplementary Material, we discuss in detail the inclusion of non-Hermitian contributions to a two-band Hamiltonian model. We compare the band broadening adopted in the main text to the *ab initio* results from Ref. [43]. In Sec. I A, we discuss the ineffective nonlocal dissipation terms and our effective area law. In Sec. I B we provide a detailed derivation of Eq. (11). Finally, we discuss the role of the purely dissipative higher-order-nearest-neighbor terms neglected in Eq. (11).

I. ADDING NON-HERMITIAN CONTRIBUTIONS

Let us consider a $2d$ magnetic system with two degrees of freedom, whose (Hermitian) dynamics is described by the following Hamiltonian:

$$\mathcal{H} = h_0\sigma_0 + h_x\sigma_x + h_y\sigma_y + h_z\sigma_z, \quad (\text{S.1})$$

where the h_i are functions of the $2d$ wavevector \mathbf{k} and σ_i ($i = 0, x, y, z$) are the Pauli matrices. The (real) eigenvalues of Eq. (S.1) are

$$E_{\text{op(ac)}}^{\text{h}} = h_0 \pm \sqrt{h_x^2 + h_y^2 + h_z^2}. \quad (\text{S.2})$$

If U is the corresponding eigenvector matrix, one can write $U^{-1}\mathcal{H}U = \mathcal{H}_d$, where $\mathcal{H}_d = \text{diag}(E_{\text{ac}}^{\text{h}}, E_{\text{op}}^{\text{h}})$ is a diagonal matrix. In order to account for the finite quasi-particle lifetime, we redefine the eigenvalues (S.2) by including an imaginary term $\Delta E_{\text{op(ac)}}$, i.e.,

$$E_{\text{op(ac)}} = h_0 \pm \sqrt{h_x^2 + h_y^2 + h_z^2} + \Delta E_{\text{op(ac)}}, \quad (\text{S.3})$$

*Electronic address: dengku@bc.edu

†Electronic address: flebus@bc.edu

with $\text{Re}E_{\text{op(ac)}} = E_{\text{op(ac)}}^{\text{h}}$. In the basis of the acoustic and optical modes with complex energies defined by Eq. (S.3), we can define a non-Hermitian Hamiltonian in the basis of its eigenvectors as $\mathcal{H}_{d,\text{nh}} = \text{diag}(E_{\text{ac}}, E_{\text{op}})$. To obtain the non-Hermitian Hamiltonian $\mathcal{H}_{d,\text{nh}}$ in the sublattice basis, we treat the non-Hermitian contribution to the Hamiltonian as a perturbation. While this procedure might not be rigorous for the parameters used in this work, it allows us to identify the general form of the Hamiltonian in the sublattice basis. One could then use the later expression to perform directly a fitting to *ab initio* or experimental data. To the leading order in the non-Hermitian perturbation, we can rewrite the non-Hermitian Hamiltonian in the sublattice basis as

$$\mathcal{H}_{\text{nh}} = U\mathcal{H}_{d,\text{nh}}U^{-1}. \quad (\text{S.4})$$

After few straightforward algebraic manipulations, we find the explicit form of Eq. (S.4) as

$$\mathcal{H}_{\text{nh}} = (h_0 + B_0)I + h_x(1 + A_0)\sigma_x + h_y(1 + A_0)\sigma_y + h_z(1 + A_0)\sigma_z, \quad (\text{S.5})$$

with

$$A_0 = \frac{\Delta E_{\text{op}} - \Delta E_{\text{ac}}}{2\sqrt{h_x^2 + h_y^2 + h_z^2}}, \quad B_0 = \frac{1}{2}(\Delta E_{\text{ac}} + \Delta E_{\text{op}}). \quad (\text{S.6})$$

Up to now, our treatment is general and it is valid in the perturbative limit. Here we specialize to the Hamiltonian described by Eq. (9) in the main text. We have included non-Hermitian terms according to Eqs. (6) and (7) in the main text in order to reproduce the trends reported in Ref. [43], in which the magnon-phonon driven band broadening of the optical (OP) mode is found to be a constant function of the wavevector \mathbf{k} , i.e., $\Delta E_{\text{op}} \propto \text{constant}$, while for the acoustic (AC) mode we have $\Delta E_{\text{ac}} \propto k^2$.

It is important to note that the model of Ref. [43] for the honeycomb lattice does not include NNN Dzyaloshinskii-Moriya D and Heisenberg exchange J_2 interactions. By plugging Eqs. (6) and (7) in the main text into Eq. (S.5) while setting $D, J_2 = 0, J = 4.5$ meV, $S = 1.5$ and $B = 0.1JS$ accordingly to Ref. [43], we fit the acoustic and optical band broadening to the data of Ref. [43] for temperature $T = 15$ K. Our fittings, shown in Fig. S1(a) and (b), leads to $\chi_2 = 6$ meV, $\chi_{11} = 2.82$ meV and $\chi_{12} = -0.415$ meV. However, these values – obtained directly from the *ab initio* calculation of Ref. [43] for $\text{Cr}_2\text{Ge}_2\text{Te}_6$ – do not yield a very strong skin effect at temperatures below the magnetic order temperature. To

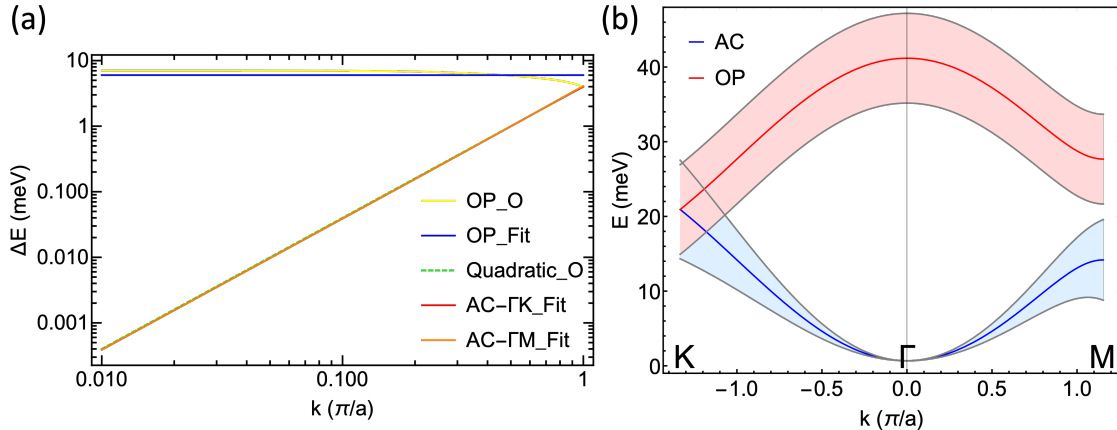


FIG. S1: (a) Band broadening ΔE on a log-log scale. The yellow (data from Ref. [43]) and blue (fitted in our model) lines indicate the broadening of the optical mode. The dashed green line (data from Ref. [43]), red line (fitted in our model, along the first Brillouin zone path $\Gamma - K$) and orange line (fitted in our model, along the first Brillouin zone path $\Gamma - M$) represent the broadening of the acoustic mode. (b) Spin-wave dispersions with associated band broadening along a representative path ($\Gamma - K - M$) in the first Brillouin zone. The blue and red lines indicate the real spectra of the acoustic and optical mode, respectively. The light blue and light red shadows represent the bands broadening of the acoustic and optical mode obtaining by fitting our model to the parameters of Ref. [43], respectively.

maximize the visibility of the skin effect, we set $J = 1.2$ meV, $S = 3/2$, $B = 0.04JS = 0.93$ T, $D = 0.8J/\sqrt{3}$, $J_2 = 0.02J$, $\chi_{11} = 1.41$ meV, $\chi_{12} = -0.415$ meV and $\chi_2 = 3$ meV. Through the main text and this supplementary material, we use these parameters if not otherwise specified.

A. Ineffective nonlocal dissipation and the effective area law

Here we show that – by setting $\chi_{12} = 0$ in Eq. (6) of the main text – the nonlocal dissipation effectively vanishes in our real space Hamiltonian model. Inverse Fourier transforming Eq. (S.5) analytically represent a challenging task due to the denominator appearing in Eq. (S.6), i.e., $\sqrt{h_x^2 + h_y^2 + h_z^2}$. Here, we adopt an approximation, i.e., we approximate each term in the denominator with its value averaged over the first Brillouin zone (BZ) and

discuss later the validity of this approximation. Let us introduce

$$\overline{h}_i^2 = \frac{1}{S_k} \int h_i^2 d^2 \mathbf{k}, \quad (\text{S.7})$$

with $i = x, y, z$ and where S_k is the area of the first BZ. Carrying out the integration (S.7) yields

$$\overline{h}_x^2 + \overline{h}_y^2 + \overline{h}_z^2 = (3J^2 + 6D^2)S^2. \quad (\text{S.8})$$

Plugging Eq. (S.8) into Eq. (S.6) leads to

$$A_0 = \frac{-i}{2S\sqrt{3(J^2 + 2D^2)}} \left[\chi_2 - \chi_{11} \left(3 - \sum_n \cos \mathbf{k} \cdot \boldsymbol{\alpha}_n \right) \right], \quad (\text{S.9})$$

$$B_0 = -\frac{i}{2} \left[\chi_2 + \chi_{11} \left(3 - \sum_n \cos \mathbf{k} \cdot \boldsymbol{\alpha}_n \right) \right]. \quad (\text{S.10})$$

Let us introduce the inverse Fourier transform of the lattice operators as

$$a_{\mathbf{k}} = \frac{1}{\sqrt{N_A}} \sum_i e^{-i\mathbf{k} \cdot \mathbf{r}_i} a_i, \quad b_{\mathbf{k}} = \frac{1}{\sqrt{N_B}} \sum_i e^{-i\mathbf{k} \cdot \mathbf{r}_i} b_i, \quad (\text{S.11})$$

where \mathbf{r}_i is the position of the i th lattice site and $N_{A(B)}$ (with $N_A = N_B$) is the total number of A(B) lattice sites. For simplicity, we separate the non-Hermitian Hamiltonian (S.5) in four components $\mathcal{H}_{\text{nh}}^m$, with $m = 1, 2, 3$, as

$$\begin{aligned} \mathcal{H}_{\text{nh}} = & \sum_{\mathbf{k}} \underbrace{(h_0 + B_0)(a_{\mathbf{k}}^\dagger a_{\mathbf{k}} + b_{\mathbf{k}}^\dagger b_{\mathbf{k}})}_{m=1} + \underbrace{h_x(1 + A_0)(a_{\mathbf{k}}^\dagger b_{\mathbf{k}} + b_{\mathbf{k}}^\dagger a_{\mathbf{k}}) + ih_y(1 + A_0)(-a_{\mathbf{k}}^\dagger b_{\mathbf{k}} + b_{\mathbf{k}}^\dagger a_{\mathbf{k}})}_{m=2} \\ & + \underbrace{h_z(1 + A_0)(a_{\mathbf{k}}^\dagger a_{\mathbf{k}} - b_{\mathbf{k}}^\dagger b_{\mathbf{k}})}_{m=3}. \end{aligned} \quad (\text{S.12})$$

Plugging Eq. (S.11) into $\mathcal{H}_{\text{nh}}^1$ leads to

$$\begin{aligned} \mathcal{H}_{\text{nh}}^1 = & \left[3JS + 6J_2S + B - \frac{i}{2}(\chi_2 + 3\chi_{11}) \right] \sum_i a_i^\dagger a_i - J_2S \sum_{\langle\langle i,j \rangle\rangle} (a_i^\dagger a_j + a_j^\dagger a_i) + a \rightarrow b \\ & + \frac{i\chi_{11}}{4N_A} \sum_{\mathbf{k}} \sum_{i,j} \sum_n \left\{ e^{i\mathbf{k} \cdot [\mathbf{r}_i - (\mathbf{r}_j + \boldsymbol{\alpha}_n)]} + e^{i\mathbf{k} \cdot [\mathbf{r}_i - (\mathbf{r}_j - \boldsymbol{\alpha}_n)]} \right\} a_i^\dagger a_j \\ = & \left[3JS + 6J_2S + B - \frac{i}{2}(\chi_2 + 3\chi_{11}) \right] \sum_i (a_i^\dagger a_i + b_i^\dagger b_i) - J_2S \sum_{\langle\langle i,j \rangle\rangle} (a_i^\dagger a_j + a_j^\dagger a_i + b_i^\dagger b_j + b_j^\dagger b_i). \end{aligned} \quad (\text{S.13})$$

Note that, in the second line, the summation over momenta $\sum_{\mathbf{k}}$ leads to $\delta_{\mathbf{r}_i, \mathbf{r}_j + \boldsymbol{\alpha}_n}$ and $\delta_{\mathbf{r}_i, \mathbf{r}_j - \boldsymbol{\alpha}_n}$. These terms vanishes because i and j label the same lattice pair, i.e., $i, j = A, A$

(B, B), while bond vector $\boldsymbol{\alpha}_n$ connects nearest-neighbors lattice sites, i.e., A and B. Thus, Eq. (S.13) reduces to

$$\mathcal{H}_{\text{nh}}^1 = \left[3JS + 6J_2S + B - \frac{i}{2}(\chi_2 + 3\chi_{11}) \right] \sum_i (a_i^\dagger a_i + b_i^\dagger b_i) - J_2S \sum_{\langle\langle i,j \rangle\rangle} (a_i^\dagger a_j + a_j^\dagger a_i + b_i^\dagger b_j + b_j^\dagger b_i). \quad (\text{S.14})$$

Plugging Eq. (S.11) into $\mathcal{H}_{\text{nh}}^2$ yields

$$\begin{aligned} \mathcal{H}_{\text{nh}}^2 &= -JS \sum_{\mathbf{k}} \sum_n (1 + A_0) (\cos \mathbf{k} \cdot \boldsymbol{\alpha}_n a_{\mathbf{k}}^\dagger b_{\mathbf{k}} + \cos \mathbf{k} \cdot \boldsymbol{\alpha}_n b_{\mathbf{k}}^\dagger a_{\mathbf{k}}) \\ &\quad + i \sin \mathbf{k} \cdot \boldsymbol{\alpha}_n a_{\mathbf{k}}^\dagger b_{\mathbf{k}} - i \sin \mathbf{k} \cdot \boldsymbol{\alpha}_n b_{\mathbf{k}}^\dagger a_{\mathbf{k}}) \\ &= -JS \sum_{\mathbf{k}} \left\{ 1 - \frac{i}{2S\sqrt{3}(J^2 + 2D^2)} \left[\chi_2 - \chi_{11} \left(3 - \sum_m \cos \mathbf{k} \cdot \boldsymbol{\alpha}_m \right) \right] \right\} \\ &\quad \times \sum_n (e^{i\mathbf{k} \cdot \boldsymbol{\alpha}_n} a_{\mathbf{k}}^\dagger b_{\mathbf{k}} + e^{-i\mathbf{k} \cdot \boldsymbol{\alpha}_n} b_{\mathbf{k}}^\dagger a_{\mathbf{k}}) \\ &= -JS \sum_{\langle i,j \rangle} \left[1 - \frac{i(\chi_2 - 3\chi_{11})}{2S\sqrt{3}(J^2 + 2D^2)} \right] (a_i^\dagger b_j + b_j^\dagger a_i). \end{aligned} \quad (\text{S.15})$$

Similarly to Eq. (S.13), the contributions from terms $\propto \sum_m \cos \mathbf{k} \cdot \boldsymbol{\alpha}_m$ vanish since they lead to terms $\propto \delta_{\mathbf{r}_i, \mathbf{r}_j - \boldsymbol{\alpha}_m - \boldsymbol{\alpha}_n}$, while i and j connect the nearest-neighbor sites A-B or B-A. Similarly, for the Hamiltonian term $\mathcal{H}_{\text{nh}}^3$ the contributions due to the term $\sum_m \cos \mathbf{k} \cdot \boldsymbol{\alpha}_m$ do not survive either. We obtain

$$\mathcal{H}_{\text{nh}}^3 = -DS \sum_{\langle\langle i,j \rangle\rangle} \left[1 - \frac{i(\chi_2 - 3\chi_{11})}{2S\sqrt{3}(J^2 + 2D^2)} \right] (i\nu_{ij} a_i^\dagger a_j - i\nu_{ij} a_j^\dagger a_i + i\nu_{ij} b_i^\dagger b_j - i\nu_{ij} b_j^\dagger b_i). \quad (\text{S.16})$$

Summing Eq. (S.14), (S.15) and (S.16) leads to

$$\begin{aligned} \mathcal{H}_{\text{nh}}^{\text{R}} &= \left[3JS + 6J_2S + B - \frac{i}{2}(\chi_2 + 3\chi_{11}) \right] \sum_i (a_i^\dagger a_i + b_i^\dagger b_i) \\ &\quad - JS \sum_{\langle i,j \rangle} \left[1 - \frac{i(\chi_2 - 3\chi_{11})}{2S\sqrt{3}(J^2 + 2D^2)} \right] (a_i^\dagger b_j + b_j^\dagger a_i) - J_2S \sum_{\langle\langle i,j \rangle\rangle} (a_i^\dagger a_j + a_j^\dagger a_i + b_i^\dagger b_j + b_j^\dagger b_i) \\ &\quad - DS \sum_{\langle\langle i,j \rangle\rangle} \left[1 - \frac{i(\chi_2 - 3\chi_{11})}{2S\sqrt{3}(J^2 + 2D^2)} \right] (i\nu_{ij} a_i^\dagger a_j - i\nu_{ij} a_j^\dagger a_i + i\nu_{ij} b_i^\dagger b_j - i\nu_{ij} b_j^\dagger b_i). \end{aligned} \quad (\text{S.17})$$

Thus, in the sublattice basis, the contribution from terms $\propto \sum_n \cos \mathbf{k} \cdot \boldsymbol{\alpha}_n$ in Eq. (S.9) and (S.10) vanishes. Thus, the resulting Hamiltonian is equivalent to the one that can be derived from the following non-Hermitian terms

$$A_0 = \frac{-i(\chi_2 - 3\chi_{11})}{2S\sqrt{3}(J^2 + 2D^2)}, \quad B_0 = -\frac{i}{2}(\chi_2 + 3\chi_{11}). \quad (\text{S.18})$$

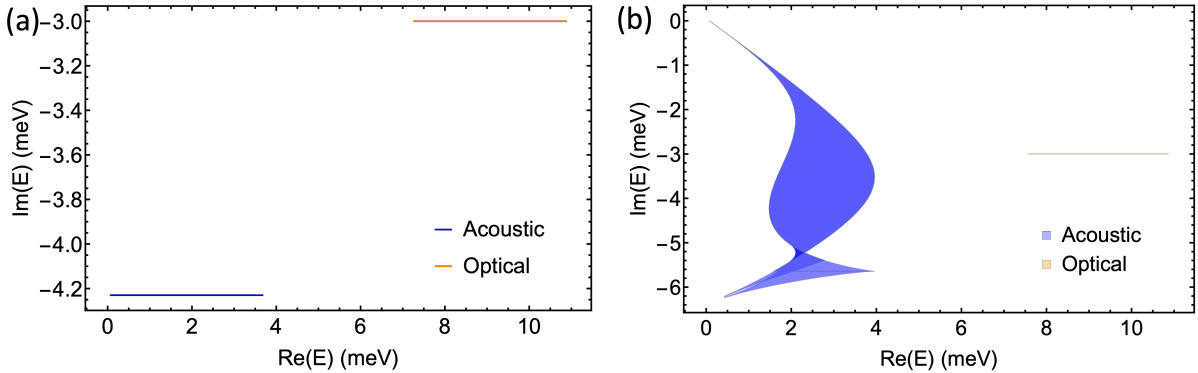


FIG. S2: (a) Effective complex energy spectra of the acoustic (blue) and optical (orange) modes for Eq. (S.18). The acoustic spectrum reduces to a line. (b) The whole acoustic (blue) and optical (orange) spectra in complex plane according to Eqs. (S.9) and (S.10) while setting $\chi_{12} = 0$. The acoustic spectra (blue) has a finite area spectral that is effectively equivalent to the blue line displayed in (a) upon inverse Fourier transformation.

The complex energy spectra associated with the non-Hermitian contribution in Eq. (S.18) are two lines, as shown in Fig. S2(a). Thus, the skin effect can not be observed at any temperature, as we have numerically verified. Fig. S2(b) shows that the spectral area of the complex spectrum corresponding to Eqs. (S.9) and (S.10) is finite, which contradicts the spectral area law proposed by Ref. [61]. Our results suggest that the spectral area law should be revised by accounting only for an “effective area” due to the non-Hermitian contribution that survive in real-space representation. Following this reasoning, in Fig. 2(a) and 2(b) of the main text, we display the spectral area associated with Eqs. (6) and (7) while subtracting the area due to the ineffective contribution $\propto -i\chi_{12} \sum_n \cos \mathbf{k} \cdot \boldsymbol{\alpha}_n$.

B. Effective nonlocal dissipation

In this section, we derive the Hamiltonian in Eq. (11) of the main text, while dropping the ineffective nonlocal dissipation term from Eqs. (6) and (7). Invoking the approximation (S.8), we can rewrite Eqs. (6) and (7) as

$$\Delta E_{ac} = -3i\chi_{11} - i\chi_{12} \left(3 - \sum_n \cos \mathbf{k} \cdot \boldsymbol{\beta}_n \right), \quad (\text{S.19})$$

$$\Delta E_{op} = -i\chi_2. \quad (\text{S.20})$$

We can generally rewrite the non-Hermitian Hamiltonian as Eq. (S.12). Inverse Fourier transforming $\mathcal{H}_{\text{nh}}^1$ leads to

$$\begin{aligned}
\mathcal{H}_{\text{nh}}^1 &= \left[3JS + 6J_2S + B - \frac{i}{2}(\chi_2 + 3\chi_{11} + 3\chi_{12}) \right] \sum_i a_i^\dagger a_i - J_2S \sum_{\langle\langle i,j \rangle\rangle} (a_i^\dagger a_j + a_j^\dagger a_i) + a \rightarrow b \\
&+ \frac{i\chi_{12}}{4N_A} \sum_{\mathbf{k}} \sum_{i,j} \sum_n \left\{ e^{i\mathbf{k}\cdot[\mathbf{r}_i - (\mathbf{r}_j + \boldsymbol{\beta}_n)]} + e^{i\mathbf{k}\cdot[\mathbf{r}_i - (\mathbf{r}_j - \boldsymbol{\beta}_n)]} \right\} a_i^\dagger a_j \\
&= \left[3JS + 6J_2S + B - \frac{i}{2}(\chi_2 + 3\chi_{11} + 3\chi_{12}) \right] \sum_i (a_i^\dagger a_i + b_i^\dagger b_i) \\
&+ \left(-J_2S + \frac{i\chi_{12}}{4} \right) \sum_{\langle\langle i,j \rangle\rangle} (a_i^\dagger a_j + a_j^\dagger a_i + b_i^\dagger b_j + b_j^\dagger b_i). \tag{S.21}
\end{aligned}$$

For the term $\mathcal{H}_{\text{nh}}^2$, we have

$$\begin{aligned}
\mathcal{H}_{\text{nh}}^2 &= -JS \sum_{\mathbf{k}} \sum_n (1 + A_0) (\cos \mathbf{k} \cdot \boldsymbol{\alpha}_n a_{\mathbf{k}}^\dagger b_{\mathbf{k}} + \cos \mathbf{k} \cdot \boldsymbol{\alpha}_n b_{\mathbf{k}}^\dagger a_{\mathbf{k}}) \\
&+ i \sin \mathbf{k} \cdot \boldsymbol{\alpha}_n a_{\mathbf{k}}^\dagger b_{\mathbf{k}} - i \sin \mathbf{k} \cdot \boldsymbol{\alpha}_n b_{\mathbf{k}}^\dagger a_{\mathbf{k}} \\
&= -JS \sum_{\langle i,j \rangle} \left[1 - \frac{i(\chi_2 - 3\chi_{11} - 3\chi_{12})}{2S\sqrt{3(J^2 + 2D^2)}} \right] (a_i^\dagger b_j + b_j^\dagger a_i) \\
&+ JS \frac{i\chi_{12}}{2S\sqrt{3(J^2 + 2D^2)}} \sum_{n,m} \frac{1}{2N_A} \sum_{i,j} \sum_{\mathbf{k}} (e^{i\mathbf{k}\cdot\boldsymbol{\beta}_m} + e^{-i\mathbf{k}\cdot\boldsymbol{\beta}_m}) \\
&\times \left[e^{i\mathbf{k}\cdot(\mathbf{r}_i - \mathbf{r}_j + \boldsymbol{\alpha}_n)} a_i^\dagger b_j + e^{i\mathbf{k}\cdot(-\mathbf{r}_i + \mathbf{r}_j - \boldsymbol{\alpha}_n)} b_j^\dagger a_i \right] \\
&= -JS \sum_{\langle i,j \rangle} \left[1 - \frac{i(\chi_2 - 3\chi_{11} - 3\chi_{12})}{2S\sqrt{3(J^2 + 2D^2)}} \right] (a_i^\dagger b_j + b_j^\dagger a_i) \\
&+ JS \frac{i\chi_{12}}{4S\sqrt{3(J^2 + 2D^2)}} \sum_{n,m} \sum_{i,j} \left\{ [\delta(\mathbf{r}_i, \mathbf{r}_j - \boldsymbol{\alpha}_n - \boldsymbol{\beta}_m) + \delta(\mathbf{r}_i, \mathbf{r}_j - \boldsymbol{\alpha}_n + \boldsymbol{\beta}_m)] a_i^\dagger b_j \right. \\
&\left. + [\delta(\mathbf{r}_i, \mathbf{r}_j - \boldsymbol{\alpha}_n + \boldsymbol{\beta}_m) + \delta(\mathbf{r}_i, \mathbf{r}_j - \boldsymbol{\alpha}_n - \boldsymbol{\beta}_m)] b_j^\dagger a_i \right\} \\
&= -JS \sum_{\langle i,j \rangle} \left[1 - \frac{i(\chi_2 - 3\chi_{11} - 2\chi_{12})}{2S\sqrt{3(J^2 + 2D^2)}} \right] (a_i^\dagger b_j + b_j^\dagger a_i) \\
&+ JS \frac{i\chi_{12}}{2S\sqrt{3(J^2 + 2D^2)}} \left(\sum_{\langle i,j \rangle^3} + \frac{1}{2} \sum_{\langle i,j \rangle^4} \right) (a_i^\dagger b_j + b_j^\dagger a_i), \tag{S.22}
\end{aligned}$$

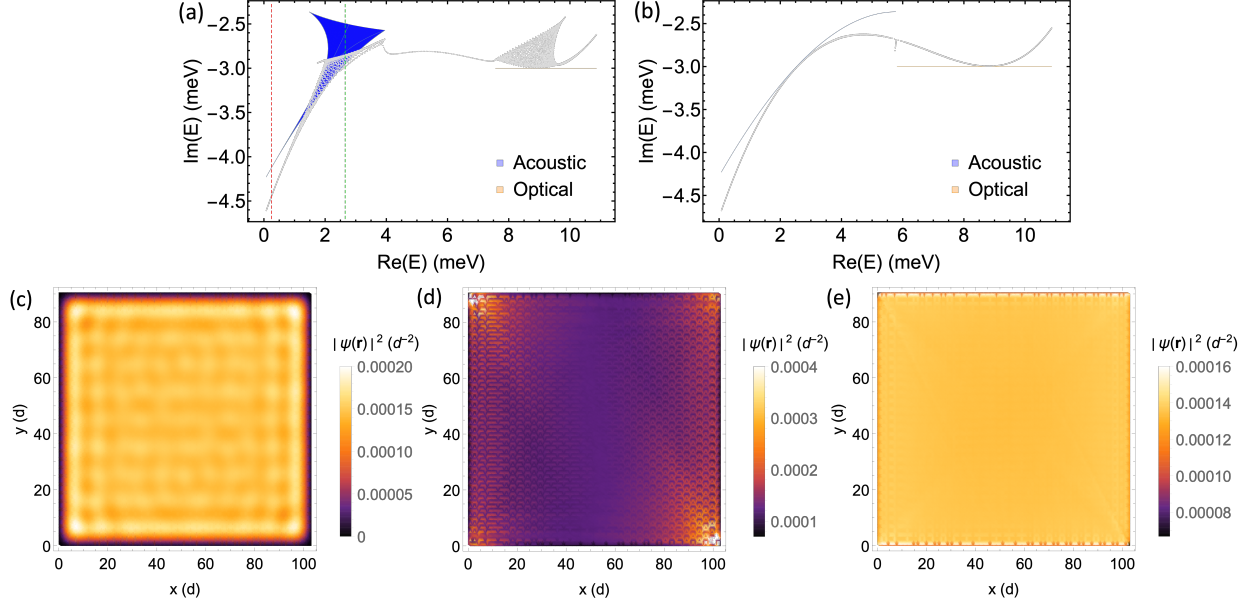


FIG. S3: (a, b) PBC spectra of the acoustic (blue) and optical (orange) modes. The OBC eigenenergies calculated from Eq. S24 are shown in light gray dots. (c-e) Spatial distribution of the density of the first N right eigenstates calculated from Eq. S24. All parameters are analogous to ones used in Fig. 2 of the main text.

where we denote $\langle i, j \rangle^n$ the n th neighbor. Finally, inverse Fourier transforming $\mathcal{H}_{\text{nh}}^3$ yields

$$\begin{aligned}
\mathcal{H}_{\text{nh}}^3 &= \sum_{\mathbf{k}} h_z (1 + A_0) (a_{\mathbf{k}}^\dagger a_{\mathbf{k}} - b_{\mathbf{k}}^\dagger b_{\mathbf{k}}) \\
&= 2DS \sum_{\mathbf{k}} \sum_n \sin \mathbf{k} \cdot \boldsymbol{\beta}_n \left\{ 1 - \frac{i[\chi_2 - 3\chi_{11} - \chi_{12}(3 - \sum_m \cos \mathbf{k} \cdot \boldsymbol{\beta}_m)]}{2S\sqrt{3}(J^2 + 2D^2)} \right\} (a_{\mathbf{k}}^\dagger a_{\mathbf{k}} - b_{\mathbf{k}}^\dagger b_{\mathbf{k}}) \\
&= -DS \sum_{\langle\langle i, j \rangle\rangle} \left[1 - \frac{i(\chi_2 - 3\chi_{11} - 3\chi_{12})}{2S\sqrt{3}(J^2 + 2D^2)} \right] i\nu_{ij} (a_i^\dagger a_j - a_j^\dagger a_i + b_i^\dagger b_j - b_j^\dagger b_i) \\
&\quad + DS \sum_{\mathbf{k}} \sum_n (e^{i\mathbf{k} \cdot \boldsymbol{\beta}_n} - e^{-i\mathbf{k} \cdot \boldsymbol{\beta}_n}) (-i) \frac{-i\chi_{12}}{2S\sqrt{3}(J^2 + 2D^2)} \frac{1}{2N_A} \sum_m (e^{i\mathbf{k} \cdot \boldsymbol{\beta}_m} + e^{-i\mathbf{k} \cdot \boldsymbol{\beta}_m}) \\
&\quad \times \sum_{i, j} e^{i\mathbf{k} \cdot (\mathbf{r}_i - \mathbf{r}_j)} (a_i^\dagger a_j - b_i^\dagger b_j)
\end{aligned}$$

$$\begin{aligned}
&= -DS \sum_{\langle\langle i,j \rangle\rangle} \left[1 - \frac{i(\chi_2 - 3\chi_{11} - 3\chi_{12})}{2S\sqrt{3}(J^2 + 2D^2)} \right] i\nu_{ij}(a_i^\dagger a_j - a_j^\dagger a_i + b_i^\dagger b_j - b_j^\dagger b_i) \\
&\quad - DS \frac{\chi_{12}}{2S\sqrt{3}(J^2 + 2D^2)} \frac{1}{2} \sum_{n,m,i,j} \left[\delta(\mathbf{r}_i, \mathbf{r}_j - \boldsymbol{\beta}_n - \boldsymbol{\beta}_m) + \delta(\mathbf{r}_i, \mathbf{r}_j - \boldsymbol{\beta}_n + \boldsymbol{\beta}_m) \right. \\
&\quad \left. - \delta(\mathbf{r}_i, \mathbf{r}_j + \boldsymbol{\beta}_n - \boldsymbol{\beta}_m) - \delta(\mathbf{r}_i, \mathbf{r}_j + \boldsymbol{\beta}_n + \boldsymbol{\beta}_m) \right] (a_i^\dagger a_j - b_i^\dagger b_j) \\
&= -DS \sum_{\langle\langle i,j \rangle\rangle} \nu_{ij} \left[i + \frac{\chi_2 - 3\chi_{11} - 2\chi_{12}}{2S\sqrt{3}(J^2 + 2D^2)} \right] (a_i^\dagger a_j - a_j^\dagger a_i + b_i^\dagger b_j - b_j^\dagger b_i) \\
&\quad - DS \frac{\chi_{12}}{2S\sqrt{3}(J^2 + 2D^2)} \sum_{\langle\langle i,j \rangle\rangle} \frac{\mu_{ij}}{2} (-a_i^\dagger a_j + a_j^\dagger a_i - b_i^\dagger b_j + b_j^\dagger b_i), \tag{S.23}
\end{aligned}$$

where $\mu_{i,j}$ connects two sites with distance of $2\boldsymbol{\beta}_n$. Denoting $\mathbf{r}_{i_M} = (\mathbf{r}_i + \mathbf{r}_j)/2$, one can set $\mu_{i,j} = \nu_{i_M,j}$. Summing together Eqs. (S.21), (S.22) and (S.23) we find

$$\begin{aligned}
\mathcal{H}_{\text{nh}}^{\text{R}} &= \left[3JS + 6J_2S + B - \frac{i}{2}(\chi_2 + 3\chi_{11} + 3\chi_{12}) \right] \sum_i (a_i^\dagger a_i + b_i^\dagger b_i) \\
&\quad + \left(-J_2S + \frac{i\chi_{12}}{4} \right) \sum_{\langle\langle i,j \rangle\rangle} (a_i^\dagger a_j + a_j^\dagger a_i + b_i^\dagger b_j + b_j^\dagger b_i) \\
&\quad - JS \sum_{\langle i,j \rangle} \left[1 - \frac{i(\chi_2 - 3\chi_{11} - 2\chi_{12})}{2S\sqrt{3}(J^2 + 2D^2)} \right] (a_i^\dagger b_j + b_j^\dagger a_i) \\
&\quad - DS \sum_{\langle\langle i,j \rangle\rangle} \nu_{ij} \left[i + \frac{\chi_2 - 3\chi_{11} - 2\chi_{12}}{2S\sqrt{3}(J^2 + 2D^2)} \right] (a_i^\dagger a_j - a_j^\dagger a_i + b_i^\dagger b_j - b_j^\dagger b_i) \\
&\quad + JS \frac{i\chi_{12}}{2S\sqrt{3}(J^2 + 2D^2)} \left(\sum_{\langle\langle i,j \rangle\rangle} + \frac{1}{2} \sum_{\langle\langle i,j \rangle\rangle^4} \right) (a_i^\dagger b_j + b_j^\dagger a_i) \\
&\quad - DS \frac{\chi_{12}}{2S\sqrt{3}(J^2 + 2D^2)} \sum_{\langle\langle i,j \rangle\rangle} \frac{\mu_{ij}}{2} (-a_i^\dagger a_j + a_j^\dagger a_i - b_i^\dagger b_j + b_j^\dagger b_i), \tag{S.24}
\end{aligned}$$

where the last two lines are higher-order-nearest-neighbor terms that do not appear explicitly in Eq. (11) of the main text. In the main text, we neglect them since, similarly to the electron-mediated spin pumping terms, one would naturally expect a dissipative interaction to have a nondissipative counterpart. This assumption does not affect qualitatively our results: as shown by Fig. S3, the complex energy spectra, and the dependence of the skin effect on DMI and temperature are comparable with the ones shown in Fig. 2 of the main text. A finally remark on our approximations [see Eqs. (S.4) and (S.8)] is in place. While these approximations might not hold for certain parameters, they allow us to derive the structure of the non-Hermitian Hamiltonian (S.24) in sublattice basis starting from our

phenomenological ansatz, i.e. Eqs. (6) and (7). Alternatively, one could avoid invoking these approximations by starting from a Hamiltonian with the structure of Eq. (S.24) and use fitting parameters to reproduce the results of Ref. [43].

Non-Hermitian skin effect in magnetic systems

Kuangyin Deng^{1,*} and Benedetta Flebus^{1,†}

¹*Department of Physics, Boston College, 140 Commonwealth Avenue, Chestnut Hill, Massachusetts 02467, USA*

Far from being limited to a trivial generalization of their Hermitian counterparts, non-Hermitian topological phases have gained widespread interest due to their unique properties. One of the most striking non-Hermitian phenomena is the skin effect, i.e., the localization of a macroscopic fraction of bulk eigenstates at a boundary, which underlies the breakdown of the bulk-edge correspondence. Here we investigate the emergence of the skin effect in magnetic insulating systems by developing a phenomenological approach to describing magnetic dissipation within a lattice model. Focusing on a spin-orbit-coupled van der Waals (vdW) ferromagnet with spin-nonconserving magnon-phonon interactions, we find that the magnetic skin effect emerges in an appropriate temperature regime. Our results suggest that the interference between Dzyaloshinskii-Moriya interaction (DMI) and nonlocal magnetic dissipation plays a key role in the accumulation of bulk states at the boundaries.

Introduction. For decades the application of topology in condensed matter has relied on the principle of the bulk-edge correspondence, according to which the edge states of a system, which appear under open boundary conditions, can be characterized by a topological invariant calculated on a Brillouin zone defined under periodic boundary conditions [1]. In some non-Hermitian systems, however, this fundamental correspondence has been found to be broken [2–15]. As a result, bulk modes can no longer be described by Bloch’s theorem as delocalized plane waves. Instead, a macroscopic number of bulk states localize at a boundary of the system, i.e., a phenomenon dubbed as the non-Hermitian skin effect.

The skin effect has been extensively investigated in one-dimensional (1d) asymmetric Su-Schrieffer-Heeger (SSH) models [4, 7, 16–20], in which the pile-up of bulk modes at one system’s edge can be understood in terms of the imbalance hopping in the left and right directions. Experimentally, the skin effect has been uncovered in photonic systems and metamaterials with judiciously engineered non-Hermitian interactions, while its observation in a naturally occurring solid-state system has not yet been reported [17, 21–24].

Magnons, i.e., the collective excitations of magnetic systems, are bosonic quasiparticles whose number is not conserved and whose dynamics is intrinsically non-Hermitian [25–30]. Their fundamental properties, including their lifetime, can be easily tuned via external fields and drives, making them promising solid-state candidates for the exploration of non-Hermitian topological phenomena [31–34]. In this Letter, we investigate the emergence of the skin effect in insulating two-dimensional (2d) magnetic systems, in which non-Hermitian terms that violate the bulk-edge correspondence arise from intrinsic spin non-conserving interactions.

The physics of dissipative interactions in magnetic systems are very complex and the effective magnon lifetime stems from a variety of spin-wave decay mechanisms, e.g., magnon-magnon, magnon-electron, and magnon-phonon interactions, and magnon scattering on extrinsic impurities. Several theoretical works have addressed [35–42]

the dissipation due to one of the aforementioned mechanisms and have provided approximate expressions for the magnon relaxation time. These expressions are, however, often given in the continuum limit and can not be readily incorporated in a lattice model, which is an essential starting point for the investigation of the skin effect. Since a comprehensive microscopic description of the magnetic dissipative dynamics within a lattice model is a particularly challenging (and yet untackled) task, here we propose a phenomenological approach that can be tested against *ab initio* or experimental data.

As a concrete example of our approach, we focus on a ferromagnetic spin-orbit-coupled insulating vdW monolayer. Recent *ab initio* studies have addressed the phonon-driven dissipation of the eigenmodes of a vdW magnetic system and calculated its behavior over a large portion of the first Brillouin zone [43]. Here, we develop a phenomenological model for the dissipative terms that is consistent with the aforementioned *ab initio* results, while respecting the symmetries of the honeycomb lattice. We find that, away from the long-wavelength limit (but below the magnetic ordering temperature), the magnetic skin effect appears, i.e., a macroscopic number of the bulk spin-wave modes accumulate at the armchair terminations of a nanoribbon. Our results show that the localization of the bulk states relies on the interference between the Dzyaloshinskii-Moriya interactions and non-local dissipative terms.

Hermitian spin model. We consider a vdW ferromagnetic monolayer whose Hermitian spin dynamics is described by the Hamiltonian

$$\begin{aligned} \mathcal{H} = & -J \sum_{\langle i,j \rangle} \mathbf{S}_i \cdot \mathbf{S}_j - J_2 \sum_{\langle\langle i,j \rangle\rangle} \mathbf{S}_i \cdot \mathbf{S}_j \\ & - B \sum_i S_i^z + D \sum_{\langle\langle i,j \rangle\rangle} \nu_{ij} \hat{\mathbf{z}} \cdot (\mathbf{S}_i \times \mathbf{S}_j), \end{aligned} \quad (1)$$

where $J > 0$ is the nearest-neighbor (NN) Heisenberg exchange, $J_2 > 0$ the next-to-nearest neighbor (NNN) exchange coupling, $B \geq 0$ the out-of-plane magnetic field, D the NNN DMI strength and $\nu_{ij} = -\nu_{ji} = \pm 1$ reflects

the non-reciprocity of the DM interactions. Far below the magnetic ordering temperature T_c , i.e., for $T \ll T_c$, and for $D \leq (J + 4J_2)/\sqrt{3}$, we can access the magnon spectrum by introducing the linearized Holstein-Primakoff transformation with respect to a uniform ground state, i.e.,

$$S_i^+ = S_i^x + iS_i^y \approx \sqrt{2S}d_i, \quad S_i^z = S - d_i^\dagger d_i, \quad (2)$$

where S is the classical spin (in units of \hbar) and d_i (d_i^\dagger) the magnon annihilation (creation) operator at the i th site, which obeys the bosonic commutation relation $[d_i, d_j^\dagger] = \delta_{ij}$. Plugging Eq. (2) into Eq. (1) and truncating the Hamiltonian beyond quadratic terms in the Holstein-Primakoff bosons, we find

$$\begin{aligned} \mathcal{H} = & (3JS + 6J_2S + B) \sum_i d_i^\dagger d_i - JS \sum_{\langle i,j \rangle} (d_i^\dagger d_j + \text{h.c.}) \\ & - J_2S \sum_{\langle\langle i,j \rangle\rangle} (d_i^\dagger d_j + \text{h.c.}) - DS \sum_{\langle\langle i,j \rangle\rangle} (i\nu_{ij} d_i^\dagger d_j + \text{h.c.}). \end{aligned} \quad (3)$$

Performing a Fourier transformation while introducing the spinor $\Psi_{\mathbf{k}} = (a_{\mathbf{k}}, b_{\mathbf{k}})$, where $a_{\mathbf{k}}$ ($b_{\mathbf{k}}$) is the Fourier transform of the magnon annihilation operator on the A (B) sublattice, Eq. (3) becomes

$$\mathcal{H} = \sum_{i=0,x,y,z} \sum_{\mathbf{k}} \Psi_{\mathbf{k}}^\dagger (h_i \sigma_i) \Psi_{\mathbf{k}}, \quad (4)$$

with

$$\begin{aligned} h_0 &= 3JS + 6J_2S + B - 4J_2S \sum_n \cos \mathbf{k} \cdot \boldsymbol{\beta}_n, \\ h_x &= -JS \sum_n \cos \mathbf{k} \cdot \boldsymbol{\alpha}_n, \\ h_y &= JS \sum_n \sin \mathbf{k} \cdot \boldsymbol{\alpha}_n, \quad h_z = 2DS \sum_n \sin \mathbf{k} \cdot \boldsymbol{\beta}_n, \end{aligned} \quad (5)$$

where the $\boldsymbol{\alpha}_n$ and $\boldsymbol{\beta}_n$ (with $n = 1, 2, 3$) are, respectively, the NN and NNN bond vectors depicted in Fig.1(a). Here and in what follows, we omit the explicit dependence of the function h_i (for $i = x, y, z$) on the wavevector \mathbf{k} .

Non-Hermitian dissipative terms. The magnon number is not conserved due to ubiquitous spin nonconserving interactions of magnons with the crystalline lattice [35–41]. Several *ab initio* studies have investigated the dissipation of magnetic eigenmodes driven by magnon-phonon interactions, modeled via finite-temperature random phonon fluctuations that modify the distance between neighboring spins [43–45]. The linewidth broadening of the acoustic, ΔE_{ac} , and optical, ΔE_{op} , eigenmodes of a magnetic honeycomb lattice have been found to scale, respectively, as $\Delta E_{\text{ac}} \propto k^2$ (with $k = |\mathbf{k}|$) and $\Delta E_{\text{op}} \propto \text{constant}$ over a large portion of the first Brillouin zone [43]. While the broadening of the optical eigenmode is a constant that can be readily incorporated

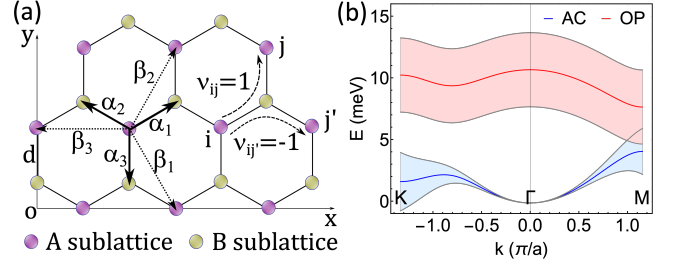


FIG. 1. (a) Ferromagnetic honeycomb lattice. $\boldsymbol{\alpha}_n$ and $\boldsymbol{\beta}_n$ are the NN and NNN bond vectors, respectively. $\nu_{ij} = 1$ and $\nu_{ij'} = -1$ label the sign of counterclockwise and clockwise DMI, respectively. (b) Spin-wave dispersions with broadening along a representative path ($\Gamma - K - M$) in the first Brillouin zone. The blue and red lines indicate the real spectra of the acoustic (AC) and optical (OP) mode, respectively. The light blue and light red shadows represent the band broadenings ΔE_{ac} and ΔE_{opt} , respectively. Here $a = \sqrt{3}d$ is the distance between A-A (B-B) sublattices, where d is the NN A-B distance.

in the lattice Hamiltonian, we cannot include the relaxation associated with the acoustic mode in the present form $\propto k^2$ as it explicitly breaks the translational symmetry of our model.

In order to reproduce the observed broadening of the acoustic eigenmode, we adopt a phenomenological approach, i.e., we include non-Hermitian terms allowed by symmetry. Our ansatz for the imaginary part of the acoustic and optical mode eigenenergies reads as

$$\begin{aligned} \Delta E_{\text{ac}} = & -i\chi_{11} \left(3 - \sum_n \cos \mathbf{k} \cdot \boldsymbol{\alpha}_n \right) \\ & -i\chi_{12} \left(3 - \sum_n \cos \mathbf{k} \cdot \boldsymbol{\beta}_n \right), \end{aligned} \quad (6)$$

$$\Delta E_{\text{op}} = -i\chi_2. \quad (7)$$

We extract the values of the parameters χ_{11} , χ_{12} and χ_2 by fitting Eqs. (6) and (7) to the *ab initio* results of Ref. [43] [46]. The band spectra and corresponding broadenings are shown in Fig. 1(b) for $\chi_{11} = 1.41$ meV, $\chi_{12} = -0.415$ meV, $\chi_2 = 3$ meV, $J = 1.2$ meV, $J_2 = 0.02J$, $S = 3/2$, $B = 0.04JS = 0.93$ T and $D = 0.8J/\sqrt{3}$. At the Γ point, the acoustic mode displays no broadening, in disagreement with ferromagnetic resonance measurements of common magnetic materials. This discrepancy most likely occurs because the analysis of Ref. [43] neglects magnon-magnon relaxation. However, we have verified that incorporating a constant dissipation term according to long-wavelength Landau-Lifshitz-Gilbert (LLG) phenomenology [47–50] does not affect qualitatively our results.

From Eqs. (4), (5), (6) and (7), the acoustic, E_{ac} , and optical, E_{op} , complex eigenenergies can be written as

$$E_{\text{ac(op)}} = h_0 \mp \sqrt{h_x^2 + h_y^2 + h_z^2 + \Delta E_{\text{ac(op)}}}. \quad (8)$$

The diagonal Hamiltonian $\mathcal{H}_d = \text{diag}(E_{\text{ac}}, E_{\text{op}})$ can be related to a non-Hermitian Hamiltonian \mathcal{H}_{nh} in the basis of the lattice operators $a_{\mathbf{k}}$ and $b_{\mathbf{k}}$ via the unitary transformation $U\mathcal{H}_dU^{-1} = \mathcal{H}_{\text{nh}}$, where U is a matrix composed of the eigenvectors of \mathcal{H} , i.e., the optical and acoustic eigenmodes of the Hermitian honeycomb lattice [51]. The Hamiltonian \mathcal{H}_{nh} can be written explicitly as

$$\mathcal{H}_{\text{nh}} = \sum_{i=0,x,y,z} \sum_{\mathbf{k}} \Psi_{\mathbf{k}}^\dagger (\tilde{h}_i \sigma_i) \Psi_{\mathbf{k}}, \quad (9)$$

where $\tilde{h}_0 = h_0 + B_0$ and $\tilde{h}_i = h_i(1 + A_0)$ for $i = x, y, z$, with

$$A_0 = \frac{\Delta E_{\text{op}} - \Delta E_{\text{ac}}}{2\sqrt{h_x^2 + h_y^2 + h_z^2}}, \quad B_0 = \frac{\Delta E_{\text{op}} + \Delta E_{\text{ac}}}{2}. \quad (10)$$

An inverse Fourier transformation yields the real-space non-Hermitian Hamiltonian as [52]

$$\begin{aligned} \mathcal{H}_{\text{nh}} = & \left[3JS + 6J_2S + B - \frac{i}{2}(\chi_2 + 3\chi_{11} + 3\chi_{12}) \right] \\ & \times \sum_i (a_i^\dagger a_i + b_i^\dagger b_i) \\ & + \left(-J_2S + \frac{i\chi_{12}}{4} \right) \sum_{\langle\langle i,j \rangle\rangle} (a_i^\dagger a_j + a_j^\dagger a_i + b_i^\dagger b_j + b_j^\dagger b_i) \\ & - JS \sum_{\langle i,j \rangle} \left[1 - \frac{i(\chi_2 - 3\chi_{11} - 2\chi_{12})}{2S\sqrt{3(J^2 + 2D^2)}} \right] (a_i^\dagger b_j + b_j^\dagger a_i) \\ & - DS \sum_{\langle\langle i,j \rangle\rangle} \nu_{ij} \left[i + \frac{\chi_2 - 3\chi_{11} - 2\chi_{12}}{2S\sqrt{3(J^2 + 2D^2)}} \right] \\ & \times (a_i^\dagger a_j - a_j^\dagger a_i + b_i^\dagger b_j - b_j^\dagger b_i) + \dots \end{aligned} \quad (11)$$

where $+\dots$ indicates purely dissipative higher-order-nearest-neighbor terms. By setting $\chi_{11,12,2} = 0$ in Eq. (11), one can recover the Hermitian Hamiltonian (3). As shown by Eq. (11), the non-Hermitian terms take the form of onsite dissipation terms and of nonlocal dissipative couplings, which resemble the well-known dissipative nonlocal coupling terms due to electron-mediated spin pumping [53, 54]. Here we retain only dissipative terms that have a non-dissipative counterpart; however, accounting for purely dissipative higher-order-nearest-neighbor terms does not affect qualitatively our results [55].

Skin effect. To investigate the breakdown of the bulk-edge correspondence and the emergence of the magnetic skin effect, we diagonalize the Hamiltonian (11) numerically under the open boundary conditions (OBC). We consider a nanoribbon with zigzag and chair terminations along, respectively, the x - and y -direction. Fig. 2(a) and 2(b) show the discrepancy between the open and periodic boundary condition (PBC) effective spectra [56], which is symptomatic of a breakdown of the

bulk-edge correspondence. From the PBC effective spectra, it is easy to see that the complex acoustic (blue) and optical (orange) bands do not cross a reference line in the complex-energy plane: thus, the system has a line gap [57, 58]. Similarly to its Hermitian counterpart, the inversion-symmetry-breaking DM interactions break the time-reversal symmetry of the magnon Hamiltonian, yielding a \mathbb{Z} topological order. Using Fukui's algorithm [59], we find $c_{\text{ac}(\text{opt})}^{\text{nB}} = \pm 1$, where c^{nB} is non-Bloch Chern number introduced by Ref. [60]. The corresponding topological magnon edge states can be clearly visualized in the real-energy-gapped region of the OBC spectrum shown in Fig. 2(a).

As a measure of the localization of the bulk eigenstates at a boundary of the ribbon, we introduce the spatial distribution $|\psi(\mathbf{r})|^2$ of the density of the first N right eigenstates $\phi_n(\mathbf{r})$ of the OBC Hamiltonian (11), i.e. [61],

$$|\psi(\mathbf{r})|^2 = \frac{1}{N} \sum_{n=1}^N |\phi_n(\mathbf{r})|^2. \quad (12)$$

Fig. 2(c) displays the spatial distribution Eq. (12) of the eigenstates with energies up to $E = 0.247$ meV (corresponding to $T \sim 2$ K with $N = 79$) [62], which is delocalized throughout the bulk. At higher energies, i.e., $E = 2.655$ meV ($T \sim 30$ K with $N = 2771$), Fig. 2(d) shows that a macroscopic number of bulk eigenstates localizes at the corners and edges the ribbon. Thus, at high enough temperature (but below the magnetic ordering temperature T_c), the skin effect appears.

The observed temperature dependence can be understood via the relation between the skin effect and spectral shape of the PBC spectra [61]. In correspondence of arc or line (finite effective spectral area) in complex energy space, the mapping from momenta to energy is $2d$ to $1d$ ($2d$): for a wave impinging at the boundary there are infinite (finite) reflection channels, and an open boundary eigenstate can (can not) be described as superposition of Bloch waves. The red and green dashed lines in Fig. 2(a) show the energies at which Fig. 2(c) and (d) are plotted, respectively. Up to $T \sim 2$ K (red line), the acoustic spectrum is (approximately) a line. Thus, the skin effect is not observable and bulk states behave as Bloch waves. This result is an agreement with the conventional long-wavelength LLG treatment of magnetic dissipation [49]. Instead, at higher energies (green line), the spectrum acquires a finite effective area and the skin effect appears.

In the absence of the DM interactions, the real and imaginary part of the energy are dependent, leading to the arc-like spectrum for both OBC and PBC displayed in Fig. 2(b). In agreement with the area law proposed by Ref. [61], the skin effect does not appear even at high temperatures, as shown in Fig. 2(e). Furthermore, in the absence of DMI, the Hamiltonian (4) becomes gapless and enters into a topologically trivial phase. Our results show that the non-reciprocity of the DM interac-

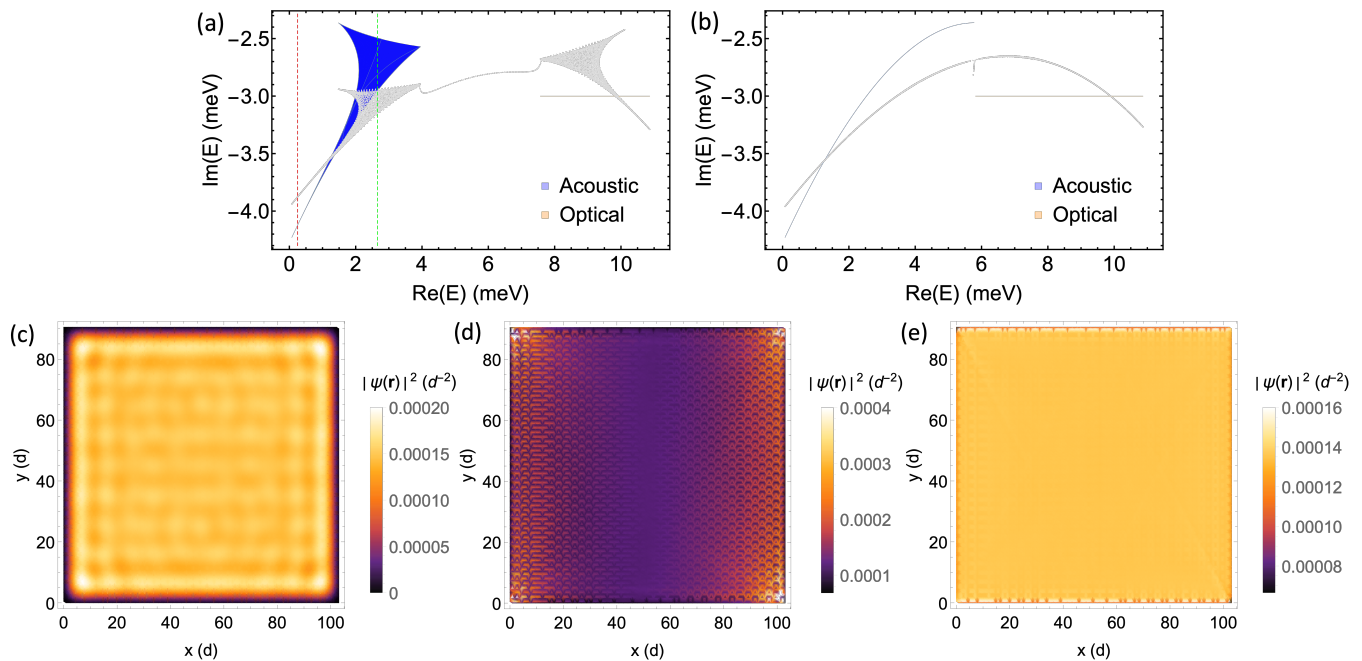


FIG. 2. (a,b) PBC spectra of the acoustic (blue) and optical (orange) modes. The OBC eigenenergies of a nanoribbon with 60×60 lattice sites are shown in light gray dots. (a) For $D = 0.8J/\sqrt{3}$. (b) For $D = 0$. (c-e) Spatial distribution of the density of the first N right eigenstates (12), (c) For $D = 0.8J/\sqrt{3}$ and $N = 79$, which corresponds to the energy $\text{Re}E = 0.247$ meV. This energy is indicated by the dashed red line in Fig. 2(a), up to which the acoustic spectrum is (approximately) a line. The skin effect is absent. (d) For $D = 0.8J/\sqrt{3}$ and $N = 2771$, which corresponds to the energy $\text{Re}E = 2.665$ meV. This energy is indicated by the dashed green line in Fig. 2(a), around which the acoustic spectrum acquires a finite effective area. The skin effect appears. (e) For $D = 0$ and $N = 2771$ there is no skin effect as the acoustic spectrum reduces to the arc shown in Fig. 2(b).

tions is essential for the emergence of both topologically nontrivial bands and of the skin effect. The skin effect in Fig. 2(d) appears to be of the first-order-type [50, 61], i.e., a macroscopic number of modes localizes at arbitrary edges due to the non-Hermitian topological properties of the Hamiltonian.

The non-locality of the magnon-phonon driven dissipation (6) plays also a key role. For $D \neq 0$ and $\chi_{12} = 0$, the skin effect does not appear even if the PBC spectrum of the acoustic eigenmode has a finite area. When $\chi_{12} = 0$, the \mathbf{k} -dependent term introducing nonlocal dissipation (6) reduces to

$$\Delta E_{\text{ac}}^{\text{nl}} = \chi_{11} \sum_n \cos \mathbf{k} \cdot \boldsymbol{\alpha}_n. \quad (13)$$

By including the nonlocal dissipation (13) in Eq. (4) and performing an inverse Fourier transformation, we find that the non-Hermitian contribution (13) vanishes in real space due to the symmetry of the honeycomb lattice [63]. Thus, the resulting real space Hamiltonian is equivalent to one derived by accounting only for the constant term $\propto -i\chi_{11}$ in Eq. (6), which yields a PBC spectrum with vanishing spectral area (i.e., a line). We have verified that in this scenario the skin effect does not appear even in the high frequency regime. This suggests that the area

law proposed by Ref. [61] should be modified in order to take into account only terms that survive upon inverse Fourier transformation and lead to a spectral area that here we call “effective”. The nonlocal contribution $\propto \chi_{12} \sum_n \cos \mathbf{k} \cdot \boldsymbol{\beta}_n$, instead, is not wiped out by lattice symmetry and, in conjunction with the DM interactions, yields the skin effect.

At a given temperature T [64], the skin effect is maximized by strong DM interactions, whose strength is proportional to the effective area of the PBC acoustic spectrum. A weak exchange coupling J leads to a reduced real-energy bandwidth of the acoustic magnon spectrum, which results in an amplified skin effect at a given frequency. The parameters χ_{11} and χ_2 lead to a featureless shift of the imaginary part of the acoustic and optical eigenenergies, respectively, while χ_{12} contributes to the spectral area. Finally, it is worth to remark that the density of right eigenstates (12) plotted in Fig. 2(c) to 2(e) might be naively interpreted as a magnon local density of states localized at an edge, which could be easily probed experimentally. However, the definition of the physical observables of non-Hermitian systems with broken bulk-edge correspondence, which are yet relatively unexplored in two and higher dimensions, require special care since they have to be defined on a biorthogonal basis and on

the real-space lattice [2, 14, 65–67]. We will address this problem in future investigations.

Discussion and outlook. In this work, we have explored the emergence of the skin effect in a spin-orbit-coupled vdW magnet. We have proposed a phenomenological approach to derive non-Hermitian Hamiltonian terms that are allowed by the symmetries of the lattice model and reproduce the band broadening observed in experimental data. We find that the skin effect appears at high enough temperatures when both nonlocal dissipative terms and DM interactions are present. Furthermore, we show that the overall temperature trend of the skin effect can be understood through spectral shape of the PBC complex energy spectrum of the acoustic magnon mode.

The dependence of the skin effect on the DM coupling, which endows the magnon bands with a nontrivial topology, suggests a connection between nontrivial band topology and $2d$ skin effect that should be investigated further. Future work should explore optimal experimental protocols to probe the localization of the bulk skin modes and address the microscopic mechanisms underlying our phenomenological model.

Finally, our approach can be easily generalized to a wide class of dissipative magnetic systems to identify a solid-state testbed of the skin effect that does not require *ad hoc* non-Hermitian engineering and whose properties can be controlled by tuning temperature and external magnetic fields.

Acknowledgments. The authors thank X. Li and E. Heinrich for insightful discussions.

* dengku@bc.edu

† flebus@bc.edu

- [1] B. A. Bernevig, *Topological insulators and topological superconductors* (Princeton university press, 2013).
- [2] F. K. Kunst, E. Edvardsson, J. C. Budich, and E. J. Bergholtz, *Physical Review Letters* **121**, 026808 (2018).
- [3] Z. Gong, Y. Ashida, K. Kawabata, K. Takasan, S. Higashikawa, and M. Ueda, *Physical Review X* **8**, 031079 (2018).
- [4] S. Yao and Z. Wang, *Physical Review Letters* **121**, 086803 (2018).
- [5] K. Yokomizo and S. Murakami, *Physical Review Letters* **123**, 066404 (2019).
- [6] C. H. Lee and R. Thomale, *Physical Review B* **99**, 201103 (2019).
- [7] F. Song, S. Yao, and Z. Wang, *Physical Review Letters* **123**, 170401 (2019).
- [8] N. Okuma and M. Sato, *Physical Review Letters* **123**, 097701 (2019).
- [9] D. S. Borgnia, A. J. Kruchkov, and R.-J. Slager, *Physical Review Letters* **124**, 056802 (2020).
- [10] N. Okuma, K. Kawabata, K. Shiozaki, and M. Sato, *Physical Review Letters* **124**, 086801 (2020).
- [11] Z. Yang, K. Zhang, C. Fang, and J. Hu, *Physical Review Letters* **125**, 226402 (2020).
- [12] C. H. Lee, L. Li, R. Thomale, and J. Gong, *Physical Review B* **102**, 085151 (2020).
- [13] C. H. Lee and S. Longhi, *Communications Physics* **3**, 1 (2020).
- [14] Y. Yi and Z. Yang, *Physical Review Letters* **125**, 186802 (2020).
- [15] L. Jin and Z. Song, *Physical Review B* **99**, 081103 (2019).
- [16] S. Longhi, *Physical Review Research* **1**, 023013 (2019).
- [17] X. Zhu, H. Wang, S. K. Gupta, H. Zhang, B. Xie, M. Lu, and Y. Chen, *Physical Review Research* **2**, 013280 (2020).
- [18] K. Xu, X. Zhang, K. Luo, R. Yu, D. Li, and H. Zhang, *Physical Review B* **103**, 125411 (2021).
- [19] L.-J. Lang, Y. Weng, Y. Zhang, E. Cheng, Q. Liang, *et al.*, *Physical Review B* **103**, 014302 (2021).
- [20] T. Hofmann, T. Helbig, F. Schindler, N. Salgo, M. Brzezińska, M. Greiter, T. Kiessling, D. Wolf, A. Vollhardt, A. Kabaši, *et al.*, *Physical Review Research* **2**, 023265 (2020).
- [21] T. Helbig, T. Hofmann, S. Imhof, M. Abdelghany, T. Kiessling, L. Molenkamp, C. Lee, A. Szameit, M. Greiter, and R. Thomale, *Nature Physics* **16**, 747 (2020).
- [22] L. Xiao, X. Zhan, Z. Bian, K. Wang, X. Zhang, X. Wang, J. Li, K. Mochizuki, D. Kim, N. Kawakami, *et al.*, *Nature Physics* **13**, 1117 (2017).
- [23] S. Weidemann, M. Kremer, T. Helbig, T. Hofmann, A. Stegmaier, M. Greiter, R. Thomale, and A. Szameit, *Science* **368**, 311 (2020).
- [24] A. Ghatak, M. Brandenbourger, J. van Wezel, and C. Coulais, *Proceedings of the National Academy of Sciences* **117**, 29561 (2020).
- [25] P. A. McClarty and J. G. Rau, *Physical Review B* **100**, 100405 (2019).
- [26] A. Galda and V. M. Vinokur, *Physical Review B* **94**, 020408 (2016).
- [27] A. Galda and V. M. Vinokur, *Scientific reports* **9**, 1 (2019).
- [28] Y. Tserkovnyak, *Physical Review Research* **2**, 013031 (2020).
- [29] T. Jeffrey, W. Zhang, and J. Sklenar, *Applied Physics Letters* **118**, 202401 (2021).
- [30] H. Liu, D. Sun, C. Zhang, M. Groesbeck, R. Mclaughlin, and Z. V. Vardeny, *Science advances* **5**, eaax9144 (2019).
- [31] B. Flebus, R. A. Duine, and H. M. Hurst, *Physical Review B* **102**, 180408 (2020).
- [32] J. Zhao, Y. Liu, L. Wu, C.-K. Duan, Y.-x. Liu, and J. Du, *Physical Review Applied* **13**, 014053 (2020).
- [33] X. Zhang, K. Ding, X. Zhou, J. Xu, and D. Jin, *Physical Review Letters* **123**, 237202 (2019).
- [34] T. Yu, Y.-X. Zhang, S. Sharma, X. Zhang, Y. M. Blanter, and G. E. Bauer, *Physical Review Letters* **124**, 107202 (2020).
- [35] S. Streib, N. Vidal-Silva, K. Shen, and G. E. Bauer, *Physical Review B* **99**, 184442 (2019).
- [36] E. Balcar, *Le Journal de Physique Colloques* **32**, C1 (1971).
- [37] X. Wu, Z. Liu, and T. Luo, *Journal of Applied Physics* **123**, 085109 (2018).
- [38] S. Rezende and R. White, *Physical Review B* **18**, 2346 (1978).
- [39] L. Berger, *Journal of Physics and Chemistry of Solids* **38**, 1321 (1977).
- [40] E. D. Thompson, *Journal of Applied Physics* **36**, 1133 (1965).
- [41] R. B. Woolsey and R. M. White, *Physical Review* **188**,

- 813 (1969).
- [42] D. Huber, in *Part A* (Springer, 1970) pp. 341–341.
- [43] K. Wang, X. Xu, Y. Cheng, M. Zhang, J.-S. Wang, H. Wang, and G. Zhang, *Applied Physics Letters* **118**, 023102 (2021).
- [44] K. Wang, J. He, M. Zhang, H. Wang, and G. Zhang, *Nanotechnology* **31**, 435705 (2020).
- [45] Y. Liu, L.-S. Xie, Z. Yuan, and K. Xia, *Physical Review B* **96**, 174416 (2017).
- [46] See Supplementary Material for more details on the fitting.
- [47] L. Landau and E. Lifshitz, *Phys. Rev* **100**, 1243 (1955).
- [48] E. Lifshitz and L. Pitaevskii, *Statistical Physics: Theory of the Condensed State*, Course of Theoretical Physics No. v. 9 (Elsevier Science, 2013).
- [49] T. L. Gilbert, *IEEE transactions on magnetics* **40**, 3443 (2004).
- [50] M. C. Hickey and J. S. Moodera, *Physical Review Letters* **102**, 137601 (2009).
- [51] See Supplementary Material for details on this derivation.
- [52] See Supplementary Material for the details on the inverse Fourier transformation.
- [53] B. Heinrich, Y. Tserkovnyak, G. Woltersdorf, A. Brataas, R. Urban, and G. E. Bauer, *Physical Review Letters* **90**, 187601 (2003).
- [54] Y. Tserkovnyak, A. Brataas, and G. E. Bauer, *Physical Review B* **67**, 140404 (2003).
- [55] See Supplementary Material.
- [56] The effective spectral area is obtained by neglecting the contribution proportional $\propto -\chi_{11} \sum_j \cos \mathbf{k} \cdot \boldsymbol{\alpha}_j$ in Eq. (6). More details on the effective area law we propose are discussed in the following main text and in the Supplementary Material.
- [57] H. Shen, B. Zhen, and L. Fu, *Physical Review Letters* **120**, 146402 (2018).
- [58] K. Kawabata, K. Shiozaki, M. Ueda, and M. Sato, *Physical Review X* **9**, 041015 (2019).
- [59] T. Fukui, Y. Hatsugai, and H. Suzuki, *Journal of the Physical Society of Japan* **74**, 1674 (2005).
- [60] S. Yao, F. Song, and Z. Wang, *Physical Review Letters* **121**, 136802 (2018).
- [61] K. Zhang, Z. Yang, and C. Fang, arXiv preprint arXiv:2102.05059 (2021).
- [62] Here we include equally-weighted contributions of magnon states up to a given energy.
- [63] See the discussion about Fig. S2 of the Supplementary Material.
- [64] Here we consider temperatures below the magnetic ordering temperature T_c , usually ~ 50 K for vdW magnets.
- [65] D. C. Brody, *Journal of Physics A: Mathematical and Theoretical* **47**, 035305 (2013).
- [66] T. Curtright and L. Mezincescu, *Journal of Mathematical Physics* **48**, 092106 (2007).
- [67] L. N. Chang, Z. Lewis, D. Minic, and T. Takeuchi, *Journal of Physics A: Mathematical and Theoretical* **46**, 485306 (2013).